Talanta 81 (2010) 643–649

Contents lists available at ScienceDirect

Talanta

journal homepage: www.elsevier.com/locate/talanta

Highly sensitive and selective fluorescence sensor based on functional SBA-15 for detection of Hg^{2+} in Aqueous Media

Chunxia Song[a], Xiaolin Zhang[a], Cuiying Jia[a], Peng Zhou[a,b,*], Xie Quan[b], Chunying Duan[a]

[a] State Key Laboratory of Fine Chemicals, Dalian University of Technology, 158 Zhongshan Road, Dalian 116012, China
[b] Key Laboratory of Industrial Ecology and Environmental Engineering (Ministry of Education), School of Environmental and Biological Science and Technology, Dalian University of Technology, Dalian 116024, China

ARTICLE INFO

Article history:
Received 21 July 2009
Received in revised form
23 December 2009
Accepted 25 December 2009
Available online 18 January 2010

Keywords:
Chemosensor
Hg^{2+}
Rhodamine B
Fluorescent probe
SBA-15

ABSTRACT

A new Rhodamine-based chemosensor **RBSN** designed for the selective detection of Hg^{2+} in aqueous media is synthesized and structural characterized. It features brightness blue emission in the presence of Hg^{2+} with the fluorescent detection limit for Hg^{2+} in aqueous media being ppb levels and exhibits excellent Hg^{2+}-specific luminescence enhancement over various competitive cations, including alkali and alkaliearth, the first-row transition metals and heavy metals. By immobilizing **RBSN** to the mesoporous **SBA-15**, a highly selective and sensitive chemosensor toward mercury cations in aqueous solution was achieved. **RBSN**/**SBA-15** could quantitatively determinate mercury cations at ppb level in the practical environmental media, suggesting the possibility for real-time quantitative detection of Hg^{2+} and the convenience for potential application in toxicological and environmental science.

1. Introduction

Mercury is one of the most concerned elements in terms of its high toxicity and high volatility [1], and its compounds have been linked with a number of human health problems, including neurological problems [2], myocardial infarction [3], and a possible involvement in the development of some kinds of autism [4]. Since the US Environmental Protection Agency (EPA) standard for the maximum allowable level of inorganic Hg^{2+} in drinking water is 2 ppb [5], the development of analytical methods for the sensitive and selective determination of mercury ion is of topical interest, especially in on-site or in situ analyses for rapid screening applications [6]. As one of the most sensitive real-time detection method, fluorometric methods have abstracted extensive attention leading to many Hg^{2+}-responsive chemosensors with fluorescence response [7]. However, much fare of the Hg^{2+} probes still has to be improved such as better water-solubility, low detect limitation and higher quantum efficiency of metal bound dyes in water [8,9].

The ordered mesoporous silica materials have attracted extensive interests as a solid support for their many advantages such as stable mesoporous structure, tunable pore size, and high specific surface area with abundant Si–OH active bonds on the pore walls [10]. Specifically, the **SBA-15** mesoporous material appears to be more attractive for its uniform channels with high surface area, better stability and large pore size (up to 30 nm) with narrow size distributions [11]. Although some fluorescent probes covalently or noncovalently bonded with mesoporous materials have been reported [12], the design and synthesis of innovative materials grafting organic functional molecules for detecting heavy metal ion are still of considerable interest, because it is crucial for environmental cleanup and also provides avenues to possible recyclability of the organic fluorophores [13,14].

Rhodamine is an ideal fluorophore that exhibits high molar extinction coefficient and high fluorescence quantum yield for detecting target molecules [15]. Recently, we reported a fluorescent probe, R6G–**SBA-15**, for detection of mercury with high sensitivity by covalent coupling of organic fluorescent molecular Rhodamine 6G within the channel of mesoporous material **SBA-15** [16]. But the influence of the strength of the interaction between organic molecule and the **SBA-15** on the photophysical and photochemical properties of the resulting materials are still not very clear, and the application of fluorescent probes need further broaden for other organic fluorescent probe which cannot be immobilized on the silicate host by covalent bond. In this paper, the new chemosensor **RBSN** was synthesized and assembled into this solid support through the intermolecular hydrogen bond, instead of covalent coupling to detect mercury ions. The spectroscopic and luminescent properties of **SBA-15** modified with **RBSN** molecules were

* Corresponding author at: State Key Laboratory of Fine Chemicals, Dalian University of Technology, 158 Zhongshan Road, Dalian 116012, China.
Tel.: +86 411 83702355; fax: +86 411 39893830.
E-mail address: zhoupeng@dlut.edu.cn (P. Zhou).

0039-9140/$ – see front matter © 2010 Elsevier B.V. All rights reserved.
doi:10.1016/j.talanta.2009.12.047

presented. Furthermore, the introduction of sulphur in **RBSN** would be in favor of improving its selectivity for mercury ions due to good sulphur-affinity character of Hg^{2+} ion. We envisioned that the metal-binding of the rhodamine fluophore would open the spirolactam ring directly and give rise to a strong fluorescence emission and color change.

2. Experimental

2.1. Reagents and instruments

Rhodamine B and 4-nitrobenzaldehyde were purchased from Aldrich. **SBA-15** was procured from Jilin University High Technology Co. Ltd. All cationic compounds such as perchlorate of Li^+, Na^+, K^+, Mg^{2+}, Ca^{2+}, Mn^{2+}, Fe^{2+}, Co^{2+}, Ni^{2+}, Cu^{2+}, Zn^{2+}, Pb^{2+}, Cd^{2+}, Hg^{2+} and Ag^+ were obtained from commercial sources and used as received. CH_3CN for spectra detection was HPLC reagent without fluorescent impurity and H_2O was deionized water. Unless otherwise stated, all the other solvents and reagents were of analytic grade and used without further purification.

The elemental analyses of C, H, N and S were performed on an Elementar varioEL III elemental analyzer. ^1H NMR and ^{13}C NMR spectra were measured on a Varian INOVA 400 M spectrometer at room temperature. The concentration of mercury in solution was measured using an Inductive Coupled Plasma Optical Emission Spectrometer (ICP-OES) (PE-Optima 2000DV). API mass spectra were recorded on HP1100LC/MSD spectrometer. ESI mass spectra were carried out on a HPLC-Q-Tof MS spectrometer using methanol as mobile phase. Uv–vis spectra were measured on a HP 8453 spectrometer. The solution fluorescent spectra were measured on Edinburgh FS920. For all fluorescent measurement, both excitation and emission slit widths were 1 nm. IR spectra were recorded using KBr pellets on a Vector 22 Bruker spectrophotometer in the 4000–400 cm^{-1} regions.

2.2. General procedures of spectra detection

Stock solution (2×10^{-2} M) of the aqueous perchlorate salts of Li^+, Na^+, K^+, Mg^{2+}, Ca^{2+}, Mn^{2+},Co^{2+}, Ni^{2+}, Cu^{2+}, Zn^{2+}, Cd^{2+}, Ag^+, Pb^{2+}, $Cu^{2+}$and Hg^{2+} were prepared. High concentration of the stock solutions **RBSN** (1.0 mM) was prepared in N,N′-dimethylformamide. Before spectroscopic measurements, the solution of RBSN was freshly prepared by diluting the high concentration stock solution to corresponding solution. The suspension solutions of **RBSN**/**SBA-15** were prepared by dispersing the fine powder in water. Each time a 2 mL solution of **RBSN** or **RBSN**/**SBA-15** was filled in a quartz cell of 1 cm optical path length, and different stock solutions of cations were added into the quartz cell gradually by using a micro-pippet. The volume of cationic stock solution added was less than 100 μL with the purpose of keeping the total volume of testing solution without obvious change. All the spectroscopic measurements were performed at least in triplicate and averaged.

2.3. Synthesis of *RBSN*

Thiooxo-rhodamine B hydrazide was synthesized according to the literature procedure [17]. 4-Nitrobenzaldehyde (0.60 mmol, 0.09 g) and thiooxo-rhodamine B hydrazide (0.4 mmol, 0.2 g) were mixed in 30 mL boiling methanol with addition of 3 drops of acetic acid. After 6 h of refluxing, red precipitates obtained were filtered off, washed with methanol/ether (1:1) and dried under vacuum. Yield: 0.18 g (81%). ^1H NMR (400 MHz, $CDCl_3$): δ 8.61 (1 H, s, CH=N), 8.22 (2 H, d, ph-H, J = 8.8 Hz), 8.13 (1 H, d, rh-H, J = 6.8 Hz), 7.93 (2 H, d, ph-H, J = 8.8 Hz), 7.46 (2 H, t, rh-H, J = 3.6 Hz), 7.16 (1 H, m, rh-H, J = 8.4 Hz), 6.75 (2H, d, rh-H, J = 8.8 Hz), 6.34 (2 H, s, rh-H), 6.30 (2 H, d, rh-H), 3.32 (8 H, m, N–CH_2, J = 13.6), 1.16 (12 H, t, –CH_3, J = 13.2); ESI-MS: m/z 606.2 for $[M+H]^+$, calc. for $[M+H]^+$, 606.2. Anal calc. for **RBSN** ($C_{35}H_{35}N_5O_3S$): H 5.82, C 69.40, N 11.56. Found: H 5.82, C 69.23, N 11.65. IR (KBr pellet, cm^{-1}): 3447s (ν_{O-H}), 2967w(ν_{C-H}), 2927w(ν_{C-H}), 1633w, 1517s ($\nu_{as\,Ar-NO_2}$), 1468w, 1426w, 1339s($\nu_{s\,CAr-N}$), 1080w.

2.4. Synthesis of hybrid mesoporous product *RBSN*/*SBA-15*

Aminopropyl functionalization (APTES) of **SBA-15** was synthesized by a similar route as in literature [18]. First, 12.5 mg of **RBSN** was dissolved in 18 mL of ethanol, and then 0.25 g of APTES/**SBA-15** was mixed in the above solution for 24 h at room temperature. The suspension was centrifuged and the transparent solution decanted. The product was filtered and washed with anhydrous ethanol, then air-dried. The resulting light pink solid powder (0.20 g) obtained was designated as **RBSN**/**SBA-15**. The concentration of **RBSN** molecule in the hybrid material was evaluated from elemental analysis of sulphur to be 0.10 mmol/g. IR (KBr pellet, cm^{-1}): 3442s (ν_{O-H}), 2968w (ν_{C-H}), 2930w (ν_{C-H}), 1632m, 1516w, 1474w, 1420w, 1338w, 1090s.

2.5. Crystallography

Crystallography intensities data of three compounds were collected on a Siemens SMART-CCD diffractometer with graphite-monochromated Mo-Kα (λ = 0.71073 Å) using the SMART and SAINT programs [19]. The structure were solved by direct methods and refined on F^2 by full-matrix least-squares methods with SHELXTL version 5.1 [20]. Crystal data of **RBSN**: $C_{35}H_{35}N_5O_3S$, M = 605.74, monoclinic, space group $P2_1/c$, black block, a = 15.415(3) Å, b = 12.176(2) Å, c = 17.791(3) Å, β = 108.536(7)°, V = 3166(1) $Å^3$, Z = 4, Dc = 1.271 g cm^{-3}, μ(Mo-Kα) = 0.146 mm^{-1}, 5579 unique reflections [Rint = 0.0573]. CCDC number 740800. Final R_1 [with $I > 2\sigma(I)$] = 0.0513, wR2 (all data) = 0.1209. Non-hydrogen atoms were refined anisotropically. Hydrogen atoms were fixed geometrically at calculated distances and allowed to ride on the parent non-hydrogen atoms, with the isotropic displacement being fixed at 1.5 times of methyl carbon atoms and 1.2 times of other carbon atoms they attached, respectively.

3. Results and discussion

The chemosensor **RBSN** was synthesized from the reaction of thiooxo-rhodamine B hydrazide and 4-nitrobenzaldehyde in methanol solution (Scheme 1) and identified by IR, elemental analyses, ^1H NMR, ESI-MS and X-ray crystal structure analyses. As shown in Fig. 1, X-ray crystallography structural investigation of **RBSN** revealed a thiospirocyclic structure with the C4S spiro ring in solid state with the torsion angle of C(8)–N(1)–N(2)–C(9) of 11.5°. The C(8)–S(1) distance of 1.734(3) Å and the C(8)=N(3) of 1.303(3) Å demonstrated the existence of a C–S single bond and a C=N double bond in the thiolactam structure. The special structure inhibited the typical emission of Rhodamine B, such that the emission of **RBSN** would be triggered and turned on when it is bound to the target thiophilic cations.

RBSN is colorless and fluorescence inactive in water–DMF (1:1, v/v) solution at pH 7, indicating that it exists in the spirocyclic form predominantly. Addition of mercuric ion to the solution of **RBSN** causes instantaneous development of a pink color and a strong yellow fluorescence. This observation shows that the mercury-induced ring-opening reaction can take place rapidly at room temperature. As we can see from Fig. 2, free **RBSN** exhibits very weak fluorescence in DMF/H_2O (1:1, v/v) when excited at

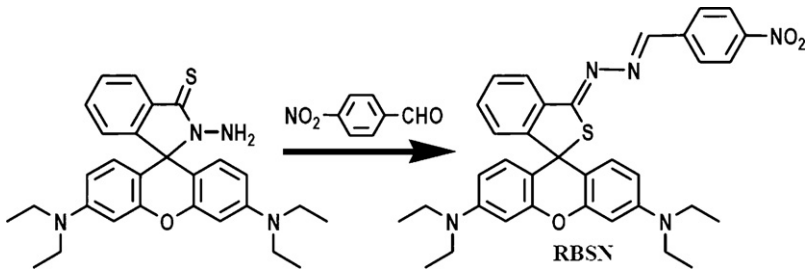

Scheme 1. Synthetic procedures of compounds **RBSN**.

500 nm. Upon the addition of Hg^{2+}, the emission band at about 600 nm appears and develops and then remains constant ($\Phi = 0.12$) with the addition of 1 equiv of Hg^{2+} ion, which can be reasonably assigned to the delocalized xanthene tautomer of the Rhodamine group [21]. After the addition of 1 equiv of mercury ions, the fluorescence intensity of the solution undergoes a *ca.* 26-Fold increase compared with that of free **RBSN** (Fig. 2). The association constant for Hg^{2+} was estimated to be $3.4 \times 10^9\ M^{-2}$ in buffer solutions on the basis of 1:2 stoichiometry.

The addition of a small amount of Hg^{2+} ion also induces a new absorption band (at 566 nm) as well as a visual color change from colorless to pink (Fig. 3). A Job's plot analysis exhibited a maximum at 0.66 mol fraction of **RBSN** (inset picture of Fig. 3), indicating the formation of 1:2 complex. To confirm the stoichiometry between **RBSN** and Hg^{2+} ion, ESI-MS analysis was conducted. Mass peaks at m/z 706.5 corresponding to $[Hg(RBSN)_2]^{2+}$ was clearly observed when 1.2 equiv of Hg^{2+} was added to **RBSN**, which gave solid evidence for the formation of a 1:2 complex.

To further explore the availability of **RBSN** as a highly selective probe for Hg^{2+}, fluorescent spectra of **RBSN** response to the other metal ions that probably affect the fluorescence intensity were examined. Changes in the fluorescence properties of **RBSN** in DMF aqueous solution caused by other metal ions, including Na^+, K^+, Mg^{2+}, Ca^{2+}, Mn^{2+}, Fe^{2+}, Co^{2+}, Ni^{2+}, Cu^{2+}, Zn^{2+}, Cd^{2+}, Pb^{2+} and Ag^+ were also measured. Only the addition of 25 mM Cu^{2+} promotes small fluorescence intensity changes and the other do not cause any significant changes under identical conditions, while addition of 5 μM Hg^{2+} into **RBSN** solution results in a dramatic change of fluorescence intensity (Fig. 4). The competition measurements were carried out by the subsequent addition of 5×10^{-4} M metal ions to the solution of **RBSN** (10 μM) in DMF/H_2O (1:1, v/v). The fluorescence spectra were recorded at 598 nm within 2 min after the addition of these metal ions and the subsequent addition of 10 equiv of Hg^{2+} to the above solutions. Fig. 5 illustrates that the enhancement in fluorescence intensity resulting from the addition of Hg^{2+} is not influenced significantly by the addition of alkali or

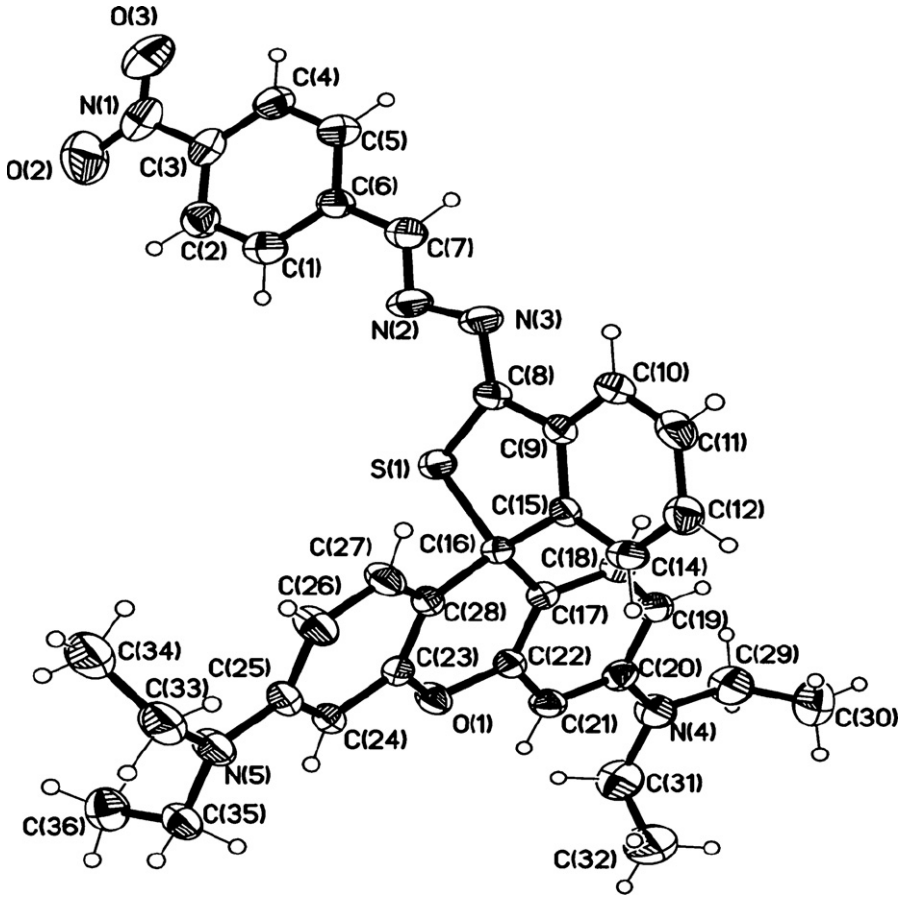

Fig. 1. Molecular structure of **RBSN** showing the atomic-numbering Thermal ellipsoids are shown at 30% probability.

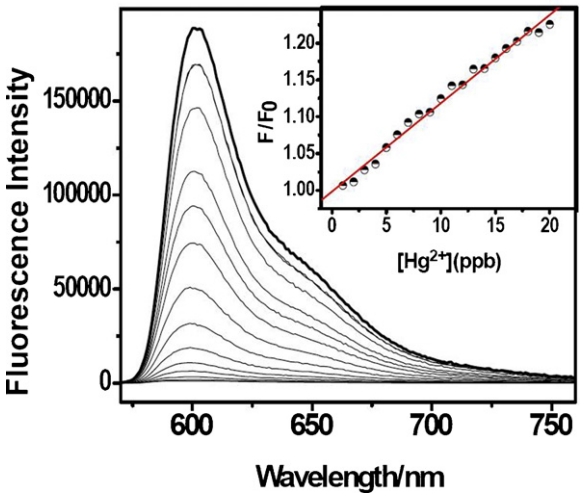

Fig. 2. Fluorescence spectral of **RBSN** (10 μM) with addition of various concentrations of Hg^{2+} at pH = 7 in DMF:H_2O = 1:1. The inset: fluorescence changes of **RBSN** (0.1 μM) upon addition of Hg^{2+} (by 1 ppb). The fluorescence intensities were measured at 598 nm. Excitation at 500 nm. Emission/excitated = 10 nm, 10 nm.

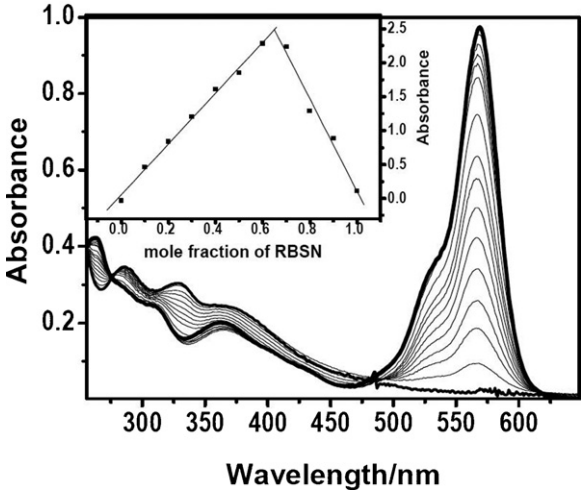

Fig. 3. Absorption spectral of **RBSN** (10 μM) with addition of various concentrations of Hg^{2+} [0, 0.05, 0.1, 0.15, 0.2, 0.25, 0.3, 0.35, 0.4, 0.5, 0.6, 0.7, 0.8, 1.0, 1.2, 1.7, 2.7, 3.7 and 5.7 equiv respectively] at pH = 7 with 0.1 mol/L KNO_3 buffer in DMF:H_2O = 1:1. Inset: Job's plots of complexation between **RBSN** and Hg^{2+} in DMF solution (DMF:H_2O = 1:1, v/v).

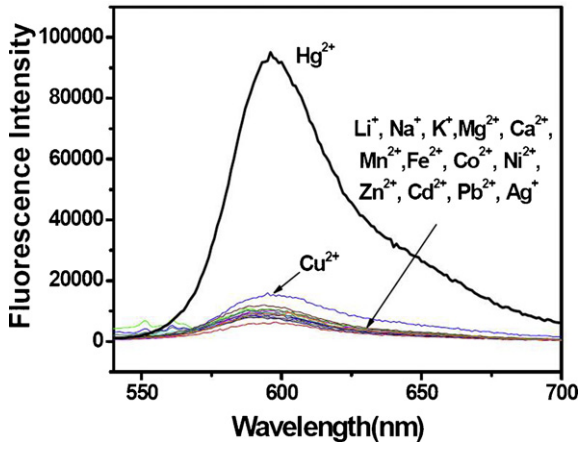

Fig. 4. Fluorescence spectra (excitation at 500 nm) of **RBSN** (5 μM) in DMF/H_2O (1:1, v/v) at pH = 7, in the presence of 50 μM Hg^{2+}, 25 mM of Li^+, Na^+, K^+, Mg^{2+}, Ca^{2+}, Mn^{2+}, Fe^{2+}, Co^{2+}, Ni^{2+}, Cu^{2+}, Ag^+, Zn^{2+}, Cd^{2+} and Pb^{2+}.

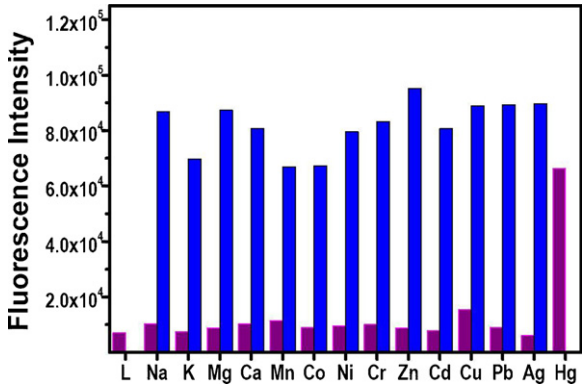

Fig. 5. The fluorescence intensity change profiles of **RBSN** (10 μM) to 50 equiv various cations in DMF/H_2O (1:1, v/v) solutions. The purple bars represent the emission intensities in the presence of Na^+, K^+, Mg^{2+}, Ca^{2+}, Mn^{2+}, Ni^{2+}, Co^{2+}, Cr^{3+}, Zn^{2+}, Cd^{2+}, Pb^{2+}, Ag^+ and Cu^{2+} respectively. The blue bars represent the emission intensities that occur upon the subsequent addition of 10 equiv of Hg^{2+} to the above mentioned solutions, respectively. Excitation was at 500 nm, and the emission intensities were integrated at 598 nm. Emission/excitated = 3 nm, 3 nm. (For interpretation of the references to color in this figure legend, the reader is referred to the web version of the article.)

alkaline-earth metals and the first-row transition metals, such as Na^+, K^+, Mg^{2+}, Ca^{2+}, Mn^{2+}, Ni^{2+}, Co^{2+}, Cr^{3+}, Zn^{2+}, Cd^{2+}, Pb^{2+}, Ag, and Cu^{2+}, respectively.

To evaluate the potential utility of **RBSN,** the influence of protons was investigated. A starting aqueous DMF solution of 10 μM probe **RBSN** (2 mL) prepared in 10 mM TRIS/HCl (or 10 mM HEPES), was used for detecting fluorescence dependence on pH upon addition of 2 μL 0.05 mol/L $Hg(NO_3)_2{\cdot}0.5\ H_2O$, and the pH of the solutions was adjusted by addition of 0.2 mol L^{-1} HCl (or 0.1 mol L^{-1} NaOH). The acid titration control experiments revealed that the titration solution did not emit any obvious and characteristic fluorescence (excitation at 500 nm) in the pH range from 4.0 to 10.0, while addition of the Hg^{2+} ion can lead to a remarkable increase of fluorescence. It shows that a suitable pH span for Hg^{2+} determination in 50% DMF aqueous solution is between pH 4 and 10.

Considering that the Environmental Protection Agency (EPA) standard for the maximum allowable level of inorganic Hg^{2+} in drinking water is 2 ppb, the limit of the chemosensor for Hg^{2+} ion has been tested. Under the experimental conditions, the fluorescence intensities of the solution of **RBSN** (0.1 μM) are nearly proportional to the amount of Hg^{2+} in DMF/H_2O (1:1, v/v) solution (2–20 ppb, R = 0.994). These results clearly show that **RBSN** can detect Hg^{2+} at the parts per billion levels under the optimized conditions.

Reversibility and regeneration are important factor for the development of devices for sensing specific analytes in practical applications [22]. In light of strong binding ability of the iodide anion (I^-) toward Hg^{2+} ion, the reversibility of the system was investigated by introduction of I^-. Colorless **RBSN** (10.0 μM in 1:1 DMF/H_2O) was first exposed to a 5 equiv of Hg^{2+} ion, then the resulting magenta solution was subsequently treated with KI (2 and 4 equiv of Hg^{2+}), which led to light-color solution. Simultaneously, new bands appeared at 256 and 300 nm (Fig. 6) are indicative of $[HgI_3]^-$ [23], that give solid evidence that the decomplexation of Hg^{2+} by I^- and followed by a spirolactam ring closure reaction to release the colorless free **RBSN**. Such reversibility is important for the fabrication of devices to sense mercuric ion.

To further realize the practical application, the chemosensor **RBSN** was anchored within the ordered one-dimensional straight channel of amine-functionalized mesoporous material **SBA-15**, to form organic–inorganic hybrid materials. This kind of receptor

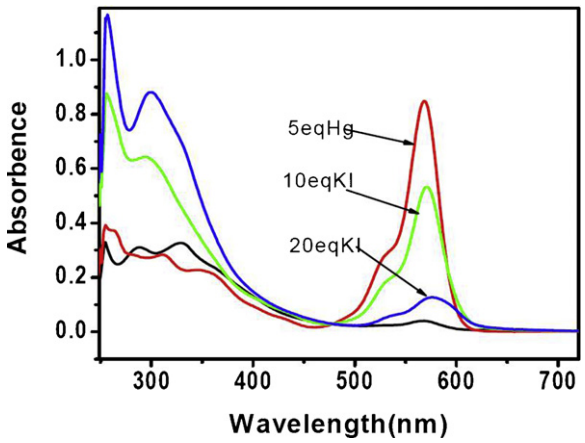

Fig. 6. Reversibility of Hg^{2+} coordination to **RBSN** (10 μM) by addition of KI (in 1:1 DMF/H_2O solution). The red line represents the absorbance enhancement that occurs immediately after the addition of 5 equiv of Hg^{2+} The green and blue lines represents the emission decreases that occur immediately after the addition of 10 and 20 equiv of KI to a solution containing the **RBSN**-Hg^{2+} complex. Bands in the UV region suggest $[HgI_3]^-$ formation. (For interpretation of the references to color in this figure legend, the reader is referred to the web version of the article.)

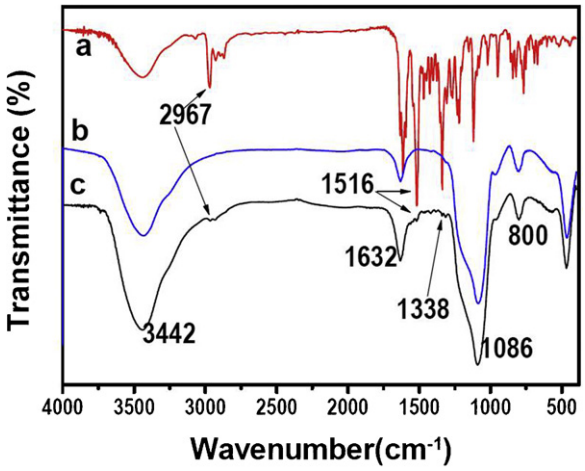

Fig. 7. IR spectra for (a) **RBSN** (red line), (b) **SBA-15** (blue line) and (c) **RBSN**/**SBA-15** (black line). (For interpretation of the references to color in this figure legend, the reader is referred to the web version of the article.)

materials as solid chemosensors can be used in heterogeneous phases and available in a chemosensory kit.

The presence of the organic ligand **RBSN** immobilized to the mesoporous **SBA-15** was characterized by IR spectra, UV–vis diffuse-reflectance spectra and fluorescence emission spectra. The IR spectra for **RBSN** (a), **SBA-15** (b) and **RBSN** functionalized hybrid mesoporous material **RBSN**/**SBA-15** (c) are shown in Fig. 7. In the spectra, the siloxane (–Si–O–Si–) bands appear as a broad strong centered at 1086 cm^{-1}(ν_{as}) and 800 cm^{-1}, while the broad peaks near 3442 and 1632 cm^{-1} are attributed to the stretching and bending vibrations of the surface silanol groups and the remaining adsorbed water molecules. The peaks in Fig. 7c near 2967 cm^{-1} is attributed to the characteristic band for asymmetric C–H stretch in $-CH_3$ and $-CH_2$ group. The new peak at 1518 cm^{-1} is assigned to anisomerous stretching vibrations of C_{Ar-NO_2}, while 1356 and 1338 cm^{-1}, are assigned to the anisomerous stretching vibrations and the symmetrical stretching vibration of C_{Ar-N} respectively. In comparison with the unmodified **SBA-15**, new peaks appeared in **RBSN**/**SBA-15** give us a solid evidence that **RBSN** is successfully grafted onto the surface of the mesoporous silica. The bands appeared in UV–vis diffuse-reflectance spectra (Fig. 8a) also disclosed the grafting of **RBSN** to **SBA-15**.

Comparing the fluorescent emission spectra of hybrid material **RBSN**/**SBA-15** and free **RBSN** coupling with Hg^{2+} (Fig. 8b), the fluorescent emission of Hg^{2+}–**RBSN** centers at 600 nm (excitation wavelength at 500 nm), and it shifts to 582 nm once the molecule is coupled to the wall of mesoporous APTES/**SBA-15**. The blue shift is attributed to the existence of abundant hydroxyl group and the nanosize pore channel of mesoporous materials, which can restrict the mobility of the π electrons in the chromophore and reduce the distance between the donor and acceptor molecules. This blue shift in photoluminescence spectra clearly shows the quantum size effects of the chemosensor.

To assess the sensing ability of the hybrid material, the UV–vis absorption spectra of the suspension solution (**RBSN**/**SBA-15** = 0.1 g/L) with different concentrations of Hg^{2+} ion was evaluated. The spectrum of **RBSN**/**SBA-15** solution does not show any absorption above 450 nm. Once Hg^{2+} ion is added, a remarkable increase in the absorption is observed in the range of 500–600 nm. The intensity near 560 nm rises with the addition of Hg^{2+} ion into the solution, suggesting the formation of the ring-opened tautomer of **RBSN** upon Hg^{2+} binding and the chemosensor **RBSN**/**SBA-15** exhibits an obvious color change from colorless to pink.

The fluorescence profile of **RBSN**/**SBA-15** upon the titration of Hg^{2+} is shown in Fig. 9, demonstrating that the limit of detection for Hg^{2+} is at the 1 ppb level. Under the experimental conditions, the fluorescence intensities of the solution of **RBSN**/**SBA-15** at 580 nm are nearly proportional to the amount of Hg^{2+} (1–13 ppb, $R = 0.995$) (Fig. 9). Adding 1 ppb of Hg^{2+} ion to a natural water (the freshwater from West Hill Reservoir, one of the water sources for Dalian) solu-

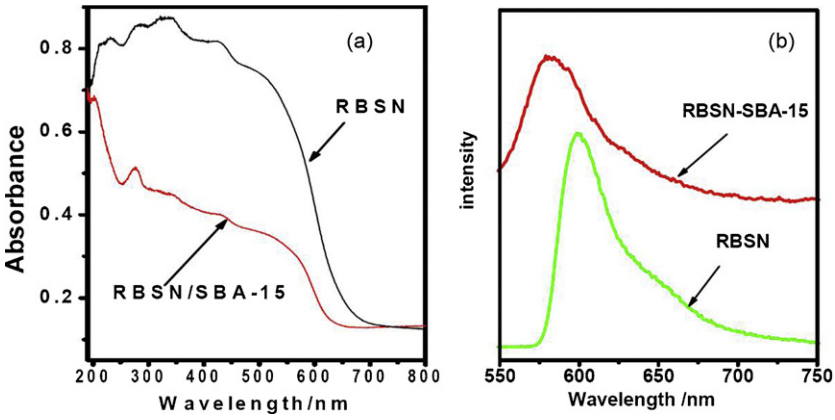

Fig. 8. (a) UV–vis diffuse-reflectance spectra of **RBSN** and **RBSN**/**SBA-15**. (b) Emission spectra of **RBSN** and **RBSN**/**SBA-15**.

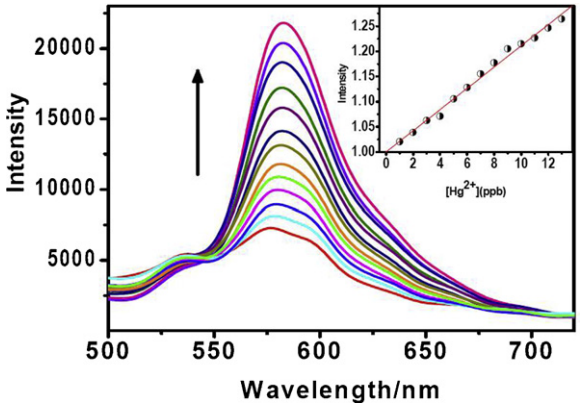

Fig. 9. Fluorescent response of **RBSN/SBA-15** (0.1 g/L) with addition of Hg^{2+} ($0–30 \times 10^{-5}$ M) in water, inset: emission intensities at 580 nm of **RBSN/SBA-15** (0.01 g/L) suspension as a function of the mercury concentration (1–13 ppb) in water. Excitation was at 500 nm.

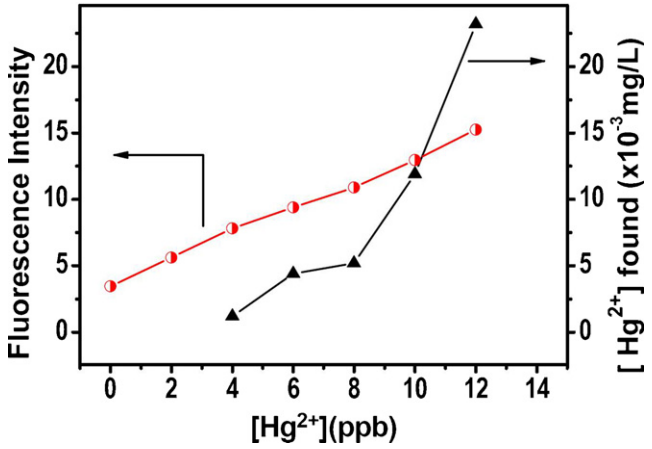

Fig. 10. Red dots: titration profile of the fluorescence spectra of **RBSN/SBA-15** (0.01 g/L) upon addition of Hg^{2+} (0–12 ppb) in 0.3% NaCl solution, emission record at 542 nm, excited at 500 nm. Black trigons: the concentration of the added Hg^{2+} determined by ICP measurement. (For interpretation of the references to color in this figure legend, the reader is referred to the web version of the article.)

tion containing **RBSN/SBA-15** affords a 70% increase of emission intensity. Despite that there are several small molecular chemosensors that have the potential to detect Hg^{2+} ion in aqueous solutions at a per billion level [24,25], **RBSN/SBA-15** is the few chemosensor that can monitor Hg^{2+} at ppb level with the fluorescent responses nearly proportional to the amount of Hg^{2+} in natural water, thus **RBSN/SBA-15** is capable of distinguishing between the safe and toxic levels of inorganic mercury in drinking water (the maximum China Standardization Administration limit for allowable levels of Hg^{2+} ions in drinking water is 1 ppb) [26] and can be used in quantitative analysis of Hg^{2+} in water.

The proposed Hg^{2+}-selective chemosensor was found to work well under laboratory conditions. Could it be used in the direct determination of mercury content in environmental sample? A typical ICP spectrometric measurement was employed to testify the accuracy of this method. For these tests, a hybrid material **RBSN/SBA-15** (0.01 g/L) in natural water with the addition of 0.3% NaCl was utilized to measure the fluorescence emission spectrum. The fluorescence intensity increased in a linear manner (Fig. 10: linearly dependent coefficient: $R^2 = 0.9982$) with the increase of the concentration of Hg^{2+}. By comparing with the ICP spectrometric measurements, the proposed chemosensor **RBSN/SBA-15** shows satisfactory result with lower detection limit and linear dependence at lower concentration of Hg^{2+}. The results obtained also indicated that the chemosensor can be applied to the determination of traces of Hg^{2+} ion in environmental samples, in the presence of co-existing cationic species (for example 0.3% Na^+) [27].

RBSN/SBA-15 was highly selective and can be regenerated by treatment with Na_2S readily. Addition of an aqueous solution of Na_2S (0.1 mM) to the natural water solutions of Hg^{2+}–**RBSN/SBA-15** species cause an immediate fluorescence decrease (Fig. 11). It demonstrates that the **RBSN/SBA-15** material may be recyclable in the environmental usage. Simultaneously, the addition of Hg^{2+} into the suspension of **RBSN/SBA-15** gives rise to a color change from colorless to pink, which means that the analytical characteristics are entirely preserved after grafting the fluorophores on the surface of **SBA-15** particles.

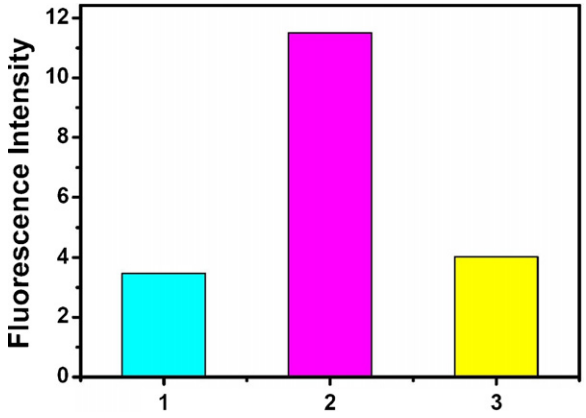

Fig. 11. Reversibility of Hg^{2+} corresponding to **RBSN/SBA-15** (0.01 g/L) in 0.3% NaCl solution by Na_2S. 1: free **RBSN/SBA-15**; 2: Hg^{2+}–**RBSN/SBA-15**; 3: Hg^{2+}–**RBSN/SBA-15** + Na_2S. Excitations were at 500 nm, and the emission intensities were integrated at 542 nm.

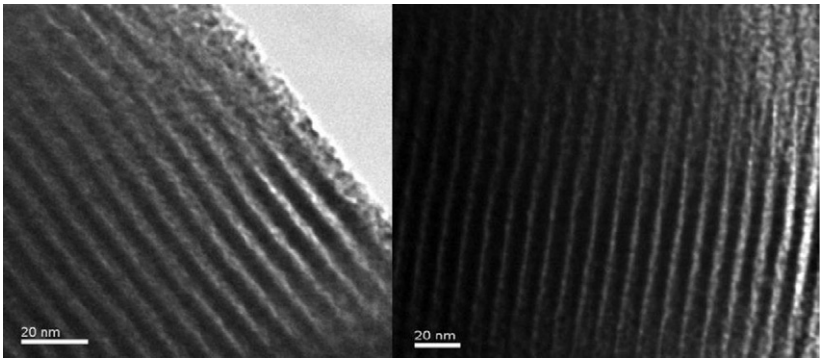

Fig. 12. TEM images in the direction perpendicular to the pore axis of (a) **SBA-15** and (b) **RBSN/SBA-15**.

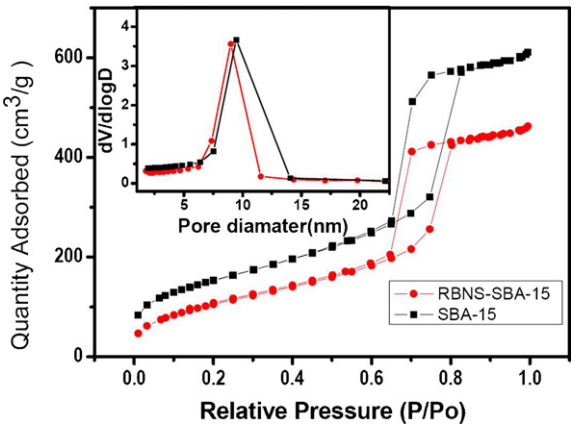

Fig. 13. Nitrogen adsorption–desorption isotherm plots and pore size distribution curves (inset) for **SBA-15** (black square) and **RBSN**/**SBA-15** (red cycle). (For interpretation of the references to color in this figure legend, the reader is referred to the web version of the article.)

To further prove that the structure of the mesoporous materials was retained after incorporation, the hybrid materials were characterized by using transmission electron microscopy (TEM), X-ray powder diffraction (XRD), nitrogen adsorption and desorption isotherms. As shown in Fig. 12, the TEM images of the hybrid material exhibit that **RBSN**/**SBA-15** displays the well-ordered one-dimensional pore structure similar to that of **SBA-15** [18], indicating that the ordered mesoporous structure of the **SBA-15** will be maintained after grafting of the functional unit.

Nitrogen physisorption measurements of the hybrid materials as well as of the **SBA-15** parent material are shown in Fig. 13. The adsorption and desorption isotherms of both materials display type IV isotherms with H1-type hysteresis loops at the high relative pressure according to the IUPAC classification, which is a characteristic of capillary condensation within uniform pores. A sharp inflection in P/P_0 range from 0.6 to 0.8 is found both on isotherms of **SBA-15** and **RBSN**/**SBA-15**, providing further proof on the maintaining of mesoporous structure after grafting [28]. The functionalized hybrid materials exhibit a considerable decrease in BET surface area, specific pore volume and pore diameter. Our results indicate that BET surface area is 559 m^2/g for **SBA-15**, but decreases to 402 m^2/g for the hybrid material, and correspondingly the pore volume shrinks to 0.73 cm^3/g from 0.97 cm^3/g for the parent material. Pore size distributions presented as a BJH plots are inserted in Fig. 13. As can be seen that the immobilization of **RBSN** decreases the pore diameters by 0.5 nm in comparison with that of parent **SBA-15**. The decrease in BET surface area, pore volume and diameters give additional proof of the grafting of the fluorescent chromophore onto the surface of the inner channel. Based on the concentration of **RBSN** on the surface (0.1 mmol/g) along with the surface area (S_{BET}) of the hybrid sensor material, the average density of the functional guests is 0.2 moleculars/nm^2. The low loadings of fluorophores could not result in aggregate formation that causes density of self-quenching of the fluorescence [29].

4. Conclusions

In summary, we have reported the new chemosensor **RBSN** which can selectively and sensitively detect Hg^{2+} in aqueous media. The ppb level fluorescent detection limit coupled in DMF/aqueous solution suggests the possibility of practical applications. By immobilizing **RBSN** to the mesoporous **SBA-15**, a highly selective and sensitive chemosensor toward mercury cations in aqueous solution was achieved. This unique hybrid inorganic/organic material is useful for the quantitative determination of Hg^{2+} at ppb levels in the practical environmental media and the method may be useful for other analytes.

References

[1] B.O. Stephan, L. Beate, R.M. Gothe, C. Beinhoff, U. Siebert, G. Drasch, Environ. Res. 107 (2008) 89.
[2] B. Weiss, T.W. Clarkson, W. Simon, Environ. Health Perspect. 110 (2002) 851.
[3] M.D. Guallar, M.I. Sanz-Gallardo, P. van't Veer, P. Bode, A. Aro, J. Gómez-Aracena, J.D. Kark, R.A. Riemersma, J.M. Martín-Moreno, F.J. Kok, N. Engl. J. Med. 347 (2002) 1747.
[4] G.N. George, R.C. Prince, J. Gailer, G.A. Buttigieg, M.B. Denton, H.H. Harris, I.J. Pickering, Chem. Res. Toxicol. 17 (2004) 999.
[5] Mercury Update: Impact on Fish Advisories. EPA Fact Sheet EPA-823-F-01-011, EPA, Office of Water, Washington, DC, 2001.
[6] H. Yang, Z. Zhou, K. Huang, M. Yu, F. Li, T. Yi, C. Huang, Org. Lett. 9 (2007) 4729.
[7] S. Yoon, E.W. Miller, Q. He, P.H. Do, C.J. Chang, Angew. Chem. Int. Ed. 46 (2007) 6658.
[8] C.-L. He, F.-L. Ren, X.-B. Zhang, Z.I.-X. Han, Talanta 70 (2006) 364.
[9] L. Guo, H. Hu, R. Sun, G. Chen, Talanta 79 (2009) 775.
[10] C.T. Kresge, M.E. Leonowicz, W.J. Roth, J.C. Vartuli, J.S. Beck, Nature 359 (1992) 710.
[11] D. Zhao, J. Feng, Q. Huo, N. Melosh, G.H. Fredrickson, B.F. Chmelka, G.D. Stucky, Science 279 (1998) 548.
[12] L. Gao, J.Q. Wang, L. Huang, X.X. Fan, J.H. Zhu, Y. Wang, Z.G. Zou, Inorg. Chem. 46 (2007) 10287.
[13] A. Stein, B.J. Melde, R.C. Schroden, Adv. Mater. 12 (2000) 1403.
[14] A.P. Wight, M.E. Davis, Chem. Rev. 102 (2002) 3589.
[15] J.-S. Wu, I.-C. Hwang, K.S. Kim, J.S. Kim, Org. Lett. 9 (2007) 907.
[16] P. Zhou, Q. Meng, G. He, H. Wu, C. Duan, X. Quan, J. Environ. Monit. 11 (2009) 648.
[17] H. Zheng, Z.-H. Qian, L. Xu, F.-F. Yuan, L.-D. Lan, J.-G. Xu, Org. Lett. 8 (2006) 859.
[18] L. Zhao, S. Wang, Y. Wu, Q. Hou, Y.J. Wang, S. Salicylidene, J. Phys. Chem. C 111 (2007) 18387.
[19] SMART and SAINT, Area Detector Control and Integration Software, Siemens Analytical X-ray Systems, Inc., Madison, WI, 1996.
[20] G.M. Sheldrick, SHELXTL V 5.1, Software Reference Manual, Bruker, AXS, Inc., Madison, WI, 1997.
[21] M.H. Lee, J.S. Wu, J.W. Lee, J.H. Jung, J.S. Kim, Org. Lett. 9 (2007) 2501.
[22] E.M. Nolan, M.E. Racine, S.J. Lippard, Inorg. Chem. 45 (2006) 2742.
[23] L. Fornaro, L. Luchini, M. Köncke, L. Mussio, E. Quagliata, K. Chattopadhyay, A. Burger, J. Cryst. Growth 217 (2000) 263.
[24] F. Song, S. Watanabe, P.E. Floreancig, K. Koide, J. Am. Chem. Soc. 130 (2008) 16460.
[25] G.K. Darbha, A.K. Singh, U.S. Rai, E. Yu, H. Yu, P.C. Ray, J. Am. Chem. Soc. 130 (2008) 8038.
[26] Standardization Administration of the People's Republic of China, Standard examination methods for drinking water—metal parameters, GB/T 5750.6-2006.
[27] W. Huang, P. Zhou, W. Yan, C. He, L. Xiong, F. Li, C. Duan, J. Environ. Monit. 11 (2009) 330.
[28] F. Zhang, Y. Yan, H. Yang, Y. Meng, C. Yu, B. Tu, D. Zhao, J. Phys. Chem. B 109 (2005) 8723.
[29] R. Méivier, I. Leray, B. Lebeau, B. Valeur, J. Mater. Chem. 15 (2005) 2965.